

Modeling Point Uncertainty in Radar SLAM

Yang Xu, Qiucan Huang, Shaojie Shen, and Huan Yin

Abstract—While visual and laser-based simultaneous localization and mapping (SLAM) techniques have gained significant attention, radar SLAM remains a robust option for challenging conditions. This paper aims to improve the performance of radar SLAM by modeling point uncertainty. The basic SLAM system is a radar-inertial odometry (RIO) system that leverages velocity-aided radar points and high-frequency inertial measurements. We first propose to model the uncertainty of radar points in polar coordinates by considering the nature of radar sensing. Then in the SLAM system, the uncertainty model is designed into the data association module and is incorporated to weight the motion estimation. Real-world experiments on public and self-collected datasets validate the effectiveness of the proposed models and approaches. The findings highlight the potential of incorporating radar point uncertainty modeling to improve the radar SLAM system in adverse environments.

Index Terms—Radar, Uncertainty modeling, Sensor fusion, SLAM

I. INTRODUCTION

KNOWING own pose is a fundamental problem for robotics as well as the navigation system. Recent state estimation techniques, such as simultaneous localization and mapping (SLAM), are widely used for pose estimation for navigation systems. Advancements in sensing technology have promoted the development and real-world deployment of visual and laser-based SLAM [1], [2], either independently or through sensor fusion approaches. These sensing modalities might fail well in adverse conditions, such as indoor fire scenes or outdoor snowy environments, thus blocking the application of robotics in these demanding situations.

Radio detection and ranging (Radar) is a robust all-weather sensing modality capable of operating effectively under challenging conditions [3], [4]. On the other hand, radar measurements are typically sparse and noisy points, which pose significant challenges for front-end data processing and back-end state estimation. To tackle this, researchers have proposed several approaches to enhance the accuracy and robustness of radar-based SLAM, such as the integration of Doppler velocity information [5] and scan-to-map matching techniques [6]. We also observe that existing radar SLAM systems often fuse radar points with inertial measurements for pose tracking, thereby advancing the utility of radar SLAM in practical robotic applications.

Generally, SLAM systems involve not only pose estimation but also uncertainty modeling. The uncertainty modeling spans from front-end measurements to back-end states, describing

the “confidence” of measurements and states. However, most existing radar SLAM systems mainly focus on motion estimation, i.e., offering sequential poses with the given input. We consider that utilizing the uncertainty of radar measurements could be a key to improving the radar SLAM performance. Thus two questions are naturally raised: *How to model the uncertainty of radar measurements?* and *How to incorporate the uncertainty modeling into a radar SLAM system effectively?*

This study tries to answer the two questions above. Specifically, we adopt our previously designed radar-inertial odometry (RIO) [7] as a reduced yet basic radar SLAM. The system takes advantage of velocity-aided radar points and high-frequency inertial measurements. Then we propose to model the uncertainty of radar points in polar coordinates by considering the nature of radar sensing. The modeled uncertainty is leveraged in both data association and weighted least squares for motion estimation. To validate the effectiveness, we conduct real-world experiments on the public Coloradar dataset [8] and our mobile platform. Overall, our key contributions in this study are summarized as follows,

- Uncertainty analyses of radar points in polar coordinates, based on the measurement model of radar sensing.
- Incorporation of the uncertainty modeling in the SLAM system, with the enhancement of designed data association and weighted residual functions.
- Ablated studies on real-world datasets demonstrate the effectiveness of the proposed modeling and approaches.

The remainder of this paper is organized as follows: Section II provides an overview of the work related to our research. In Section III, we detail the RIO system, encompassing an overview of the system, the methodology for uncertainty modeling, and the approaches applied in the estimation system. Subsequently, Section IV presents ablation studies and real-world validation on two distinct datasets. We conclude with a summary of our findings in Section V.

II. RELATED WORK

A. Uncertainty modeling in SLAM

Uncertainty is a fundamental term in SLAM. The modeled uncertainty could be used for various SLAM-related topics, such as active SLAM [9], motion detection in dynamic environments [10], lidar-camera fusion for reconstruction [11], and improving RGB-D SLAM [12].

Modeling the uncertainty is the prior condition before we could leverage it into SLAM systems. Typical SLAM systems are based on the Gaussian assumption [13], [14], hence the uncertainty is associated with the covariance matrix. Visual sensing and perception are generally data-rich, and neural networks could be trained to estimate the covariance matrices.

Yang Xu and Qiucan Huang contributed equally to this study.

All authors are with the Cheng Kar-Shun Robotics Institute, The Hong Kong University of Science and Technology, Hong Kong SAR.

This work was supported in part by the HKUST-DJI Joint Innovation Laboratory, and the Hong Kong Center for Construction Robotics (InnoHK center supported by Hong Kong ITC).

Shan *et al.* [15] propagated such uncertainty into the visual-inertial odometry. In the object SLAM system by Merrill *et al.* [16], the uncertainty was estimated by trained neural networks and utilized for outlier rejection.

Increased interests are shown in the covariance estimation in recent LiDAR-inertial odometry (LIO) systems. Considering that data-driven range sensing is not so mature, related studies mainly focus on handcrafted covariance estimation. Yuan *et al.* [17] designed a LiDAR-based voxel mapping scheme, in which a plane-based uncertainty model is proposed in discrete voxels. The experimental results demonstrate that using the uncertainty model could improve the mapping precision. In the work proposed by Jiang *et al.* [2], the uncertainty is quantified on point-based tree structures without space discretization, making it applicable to uneven laser point clouds. The tree structure is built on the nearest neighbor search LiDAR points. Our work is inspired by these existing studies. Though LiDAR and radar are both range sensings, measurements from system-on-chip radar are generally sparser than those from LiDAR sensors. Thus, directly applying existing uncertainty modeling of dense LiDAR points is inappropriate.

B. Radar SLAM for Motion Estimation

Radar-based SLAM has a long history, dating back to the late 20th century [18]. While radar is robust in all types of weather, it is often noisy and sparse, bringing difficulties to the state estimation for robotics. To address this, recent studies have suggested combining radar data with high-frequency inertial data to enhance both robustness and accuracy. Doer and Trommer [19] used an Extended Kalman Filter (EKF) for their RIO system. Kramer *et al.* [5] proposed to fuse the sensor data via sliding-window optimization, and the Doppler velocity of radar was also considered. Michalczyk *et al.* [20], [21] designed a multi-state and tightly-coupled system, in which radar points served as landmarks for data matching. In 4D iRIOM [6], Doppler velocity was used to filter out radar noise, and a technique common in LiDAR SLAM, known as distribution-to-multi-distribution matching, was developed for estimating motion. Differently, Lu *et al.* [22] introduced a data-driven-based scheme for sensor fusion. Most of the work mentioned above mainly focuses on motion estimation by regarding radar data as 3D points without considering the uncertainty of measurements. In this study, we point out that modeling the point uncertainty could help improve the radar SLAM performance.

III. METHODOLOGY

This section presents the methodology of our proposed system, organized as follows: Section III-A provides an overview of the system, including the problem formulation. In Section III-B, we address the modeling of uncertainty in radar measurements, identifying sources of noise and developing a model to accurately represent this uncertainty. In Sections III-C, III-D and III-E, we leverage the modeled uncertainty into the system for performance improvement.

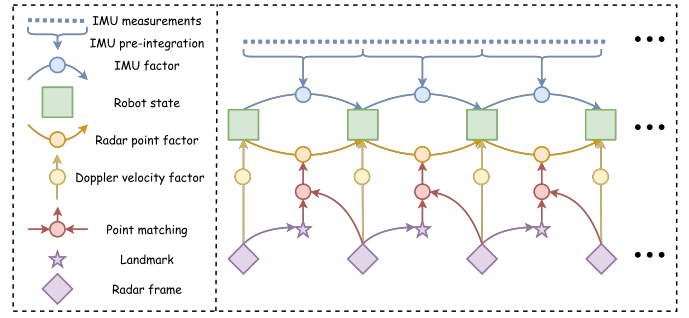


Fig. 1. Factor graph representation of our radar-inertial odometry. Three factors are constructed from the input radar and IMU measurements. Our system provides not only the estimated poses for pose estimation but also the radar landmarks as mapping results.

A. System Overview

We follow the classical sliding window-based approach to build the SLAM system [1]. The complete state of our system is defined as follows:

$$\begin{aligned} \mathbf{X} &= [\mathbf{x}_0^T, \mathbf{x}_1^T, \dots, \mathbf{x}_k^T, \mathbf{l}_0^T, \mathbf{l}_1^T, \dots, \mathbf{l}_n^T]^T \\ \mathbf{x}_i &= [\mathbf{p}_i^T, \mathbf{q}_i^T, \mathbf{v}_i^T, \mathbf{b}_{a_i}^T, \mathbf{b}_{g_i}^T]^T, \quad i \in [0, k] \\ \mathbf{l}_j &\in \mathbb{R}^3, \quad j \in [0, n] \end{aligned} \quad (1)$$

in which \mathbf{p}_i , \mathbf{q}_i and \mathbf{v}_i represent the position, rotation, and velocity of the i -th frame, respectively. The terms \mathbf{b}_{a_i} , \mathbf{b}_{g_i} denote the accelerometer bias and gyroscope bias in the i -th frame from inertial measurement unit (IMU). The term \mathbf{l}_j is the j -th map landmark.

The entire system is formulated as an optimization problem that aims to minimize a set of residuals assigned with a Mahalanobis norm, enabling the motion estimation:

$$\min_{\mathbf{X}} \left\{ \sum_{k \in I} \|\mathbf{r}_I(\mathbf{x}_k, \mathbf{x}_{k+1})\|_{\Sigma_k^{k+1}} + \sum_{k \in D} \|\mathbf{r}_D(\mathbf{x}_i, p_k)\|_{\Sigma_k} + \sum_{k \in P} \|\mathbf{r}_P(\mathbf{x}_i, \mathbf{l}_k, p_k)\|_{\Sigma_k} \right\} \quad (2)$$

where p represents a radar point. The terms $\mathbf{r}_I(\cdot)$, $\mathbf{r}_D(\cdot)$ and $\mathbf{r}_P(\cdot)$ are three different residuals. $\|\cdot\|_{\Sigma}$ presents for the Mahalanobis norm. Figure 1 presents the factor graph-based visualization of the system.

The first residual term, $\mathbf{r}_I(\cdot)$, is the IMU propagation for estimating continuous radar states. It provides an initial guess for optimizing the entire system. To avoid the time-consuming process of re-propagation, we have adopted the IMU pre-integration technique, following the approach outlined in [1]. The residual is defined as follows:

$$\mathbf{r}_I(\mathbf{x}_k, \mathbf{x}_{k+1}) = \begin{bmatrix} \mathbf{R}_k^T (\mathbf{p}_{k+1} - \mathbf{p}_k + \frac{1}{2} g \Delta t^2 - \mathbf{v}_k \Delta t) - \Delta \mathbf{p}_{k+1}^k \\ 2[\mathbf{q}_k^{-1} \otimes \mathbf{q}_{k+1} \otimes \Delta \mathbf{q}_{k+1}^k]_{xyz} \\ \mathbf{R}_k^T (\mathbf{v}_{k+1} + g \Delta t - \mathbf{v}_k) - \Delta \mathbf{v}_{k+1}^k \\ \mathbf{b}_{a_{k+1}} - \mathbf{b}_{a_k} \\ \mathbf{b}_{g_{k+1}} - \mathbf{b}_{g_k} \end{bmatrix} \quad (3)$$

where $[\cdot]$ extract the vector part of quaternion and the symbol \otimes denotes the Hamilton product. $\Delta \mathbf{p}_{k+1}^k$, $\Delta \mathbf{q}_{k+1}^k$ and $\Delta \mathbf{v}_{k+1}^k$

are results of IMU pre-integration. Δt is the time duration between two scans. Gravity, denoted as g , is assumed to align with the z -axis. We use the Mahalanobis norm to further weigh the IMU residual considering the uncertainty of propagation. Details about the covariance propagation process are the same as [1] which is omitted here for clarity.

An IMU-only dead-reckoning system could not guarantee the accuracy and reliability for robotic motion estimation. Thus we also propose to leverage radar sensing into the optimization, resulting in the other two residual terms $\mathbf{r}_D(\cdot)$ and $\mathbf{r}_P(\cdot)$ that will be introduced in the subsequent Section III-C, Section III-D and Section III-E, respectively.

B. Radar Measurement Model

Before detailing the precise formulation of radar-based residuals, it is essential to address the modeling of radar measurement and its noise. This modeling enables us to understand the inherent uncertainty associated with radar measurements, thereby improving the accuracy of motion estimation through the adjustment of residual weights.

Radar sensors emit observations as azimuth and elevation angles, along with the detected range, thus employing polar coordinate measurement models offers a more accurate formulation of error distributions, as discussed in the previous study [23]. Given a radar point ${}^R p_k$ in the radar frame R , we decompose ${}^R p_k$ to two distinct components: the range, represented by $r_k \in \mathbb{R}$, and the azimuth and elevation angles, denoted as $\Omega_k \in \mathbb{S}^2$, states as follows:

$${}^R p_k = [r_k, \Omega_k]^T \quad (4)$$

Regarding the range measurement noise, it can be modeled as a normal distribution with a mean of zero and a standard deviation of σ_r , indicated as: $\delta_{r_k} \sim \mathcal{N}(0, \sigma_r^2)$. Specifically, σ_r is the standard deviation of the range measurement noise, encapsulating the variability of the distance measurements around their true value within the defined confidence interval. Then the ground-truth range can be expressed as:

$$r_k^{gt} = r_k + \delta_{r_k} \quad (5)$$

For the angular measurement noise, we model the azimuth and elevation noise as independent Gaussian distributions centered around zero with standard deviations. Thus the angular measurement noise of Ω is expressed as: $\delta_{\Omega_k} \sim \mathcal{N}(\mathbf{0}_{2 \times 1}, \Sigma_{\Omega})$. The term Σ_{Ω} is the covariance matrix for the angular measurements:

$$\Sigma_{\Omega} = \begin{bmatrix} \sigma_{\theta}^2 & 0 \\ 0 & \sigma_{\phi}^2 \end{bmatrix} \quad (6)$$

where σ_{θ} and σ_{ϕ} are the standard deviations of the measurement noise for azimuth and elevation, respectively.

With the utilization of the \boxplus operation, which is encapsulated in \mathbb{S}^2 as described in [24], we can build the connection between the actual bearing direction Ω_k^{gt} and its corresponding measurement Ω_k as follows:

$$\Omega_k^{gt} = \Omega_k \boxplus_{\mathbb{S}^2} \delta_{\Omega_k} \triangleq e^{(\mathbf{N}(\Omega_k) \delta_{\Omega_k})^{\wedge}} \Omega_k \quad (7)$$

in which the term $\mathbf{N}(\Omega_k) = [\mathbf{N}_1 \ \mathbf{N}_2] \in \mathbb{R}^{3 \times 2}$ represents an orthonormal basis, denoted as $\mathbf{N}(\Omega_k)$, of the tangent plane

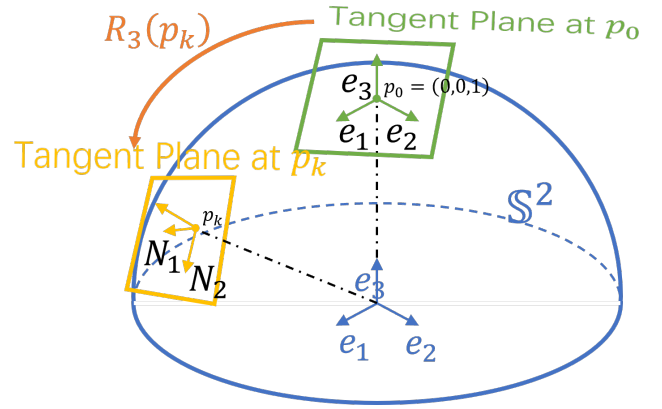


Fig. 2. To obtain the orthonormal basis $(\mathbf{N}_1, \mathbf{N}_2)$ in the tangent plane of $p_k \in \mathbb{S}^2$. $R_3(p_k)$ is defined by rotating e_3 to p_k , \mathbf{N}_1 and \mathbf{N}_2 are obtained through rotating e_1 and e_2 by $R_3(p_k)$ respectively.

at Ω_k . This can be visualized in Figure 2. In addition, the notation $(\cdot)^{\wedge}$ refers to the skew-symmetric matrix that maps the cross product. The $\boxplus_{\mathbb{S}^2}$ operation involves rotating the unit vector Ω_k around the axis δ_{Ω_k} within the tangent plane at Ω_k . This operation ensures that the resulting vector remains on the surface of \mathbb{S}^2 .

With the analyses above, given a radar point ${}^R p_k$ in polar coordinate, its true value ${}^R p_k^{gt}$ is formulated as follows:

$$\begin{aligned} {}^R p_k^{gt} &= r_k^{gt} \Omega_k^{gt} \\ &= (r_k + \delta_{r_k}) (\Omega_k \boxplus_{\mathbb{S}^2} \delta_{\Omega_k}) \\ &\approx \underbrace{r_k \Omega_k}_{{}^R p_k} + \underbrace{\Omega_k \delta_{r_k} - r_k (\Omega_k)^{\wedge} \mathbf{N}(\Omega_k) \delta_{\Omega_k}}_{{}^R \mathbf{n}_k} \end{aligned} \quad (8)$$

in which the term ${}^R \mathbf{n}_k$ represents the noise of this radar point measurement:

$${}^R \mathbf{n}_k = \underbrace{\begin{bmatrix} \Omega_k & r_k (\Omega_k)^{\wedge} \mathbf{N}(\Omega_k) \end{bmatrix}}_{\mathbf{A}_k} \begin{bmatrix} \delta_{r_k} \\ \delta_{\Omega_k} \end{bmatrix} \sim \mathcal{N}(\mathbf{0}, {}^R \Sigma_k) \quad (9)$$

and covariance of this radar point ${}^R \Sigma_k$ can be formulated as follows:

$${}^R \Sigma_k = \mathbf{A}_k \begin{bmatrix} \sigma_r^2 & \mathbf{0}_{1 \times 2} \\ \mathbf{0}_{2 \times 1} & \Sigma_{\Omega} \end{bmatrix} \mathbf{A}_k^T \quad (10)$$

To this end, we have modeled the radar measurement and its noise on range and angles, i.e., the uncertainty modeling of one radar point. In the following sections, we omit the frame R in the representations that are related to the radar point.

One might argue that radar sensing provides not only range and angles but also Doppler velocities. The uncertainty modeling of Doppler velocity is also a potential point to improve the motion estimation system. However, Doppler velocity measurements usually contain non-Gaussian noise [5], thus modeling noise as a Gaussian white noise will lead to inaccuracy results. Additionally, documentation on data accuracy indicates that Doppler velocity measurements are relatively precise, leading to our decision to omit Doppler velocity noise in this study.

C. Uncertainty-aware Residual on Doppler Velocity

Fusing Doppler velocity measurements is indispensable when the device works at a relatively high speed since it could reduce the error of IMU propagation. The Doppler velocity measurements reported by the radar should be the same as the projection of relative velocity between the radar and the object onto the direction vector of detection in the ideal scenario. This gives us the residual term $\mathbf{r}_D(\cdot)$ by fusing the Doppler velocity measurements.

$$\mathbf{r}_D(\mathbf{x}_i, p_k) = \frac{p_k^T}{\|p_k\|} \cdot \mathbf{R}_E^T (\mathbf{R}_i^T \mathbf{v}_i + (\hat{\omega}_i - \mathbf{b}_{gt})^\wedge \mathbf{t}_E) - v_{dk} \quad (11)$$

where p_k is the radar measurement in the i -th radar scan under a Cartesian coordinate system with the radar origin as its origin point; v_{dk} is the Doppler velocity of p_k ; \mathbf{R}_E and \mathbf{t}_E denote the extrinsic rotation and translation from the radar to the IMU, respectively.

Directly fusing the residuals in Equation 2 without weighting will result in a deviation of the odometry estimation, as different residuals “contribute” differently to the motion estimation. Setting pre-defined weights may improve the results to some extent, however, we argue that the significance of each point measurement differs due to the physical properties of radar sensing. As depicted in Figure 5, the uncertainty of a closer point is generally lower than that of a point located farther away. Taking this into consideration, we utilize the uncertainty model described in Section III-B to assign weights to the residuals based on their associated uncertainty levels. This approach allows for a more accurate fusion of the residuals and mitigates the impact of less reliable measurements on the overall odometry estimation.

According to the Equation 11, we integrate the noise term \mathbf{n}_k , resulting in the following formulation:

$$0 = \frac{(p_k + \mathbf{n}_k)^T}{\|p_k + \mathbf{n}_k\|} \cdot \underbrace{\mathbf{R}_E^T (\mathbf{R}_i^T \mathbf{v}_i + (\hat{\omega}_i - \mathbf{b}_{gt})^\wedge \mathbf{t}_E)}_{\mathbf{K} \in \mathbb{R}^{3 \times 1}} - v_{dk} \quad (12)$$

$$\approx \mathbf{r}_D(\mathbf{x}_i, p_k) + \mathbf{J}_{\mathbf{n}_k} \mathbf{n}_k$$

where $\mathbf{r}_D(\cdot)$ is the residual of Doppler velocity, \mathbf{n}_k is the noise of radar point measurement and $\mathbf{J}_{\mathbf{n}_k}$ can be represented as follows:

$$\mathbf{J}_{\mathbf{n}_k} = \frac{\partial \mathbf{d}}{\partial \mathbf{n}_k} \cdot \mathbf{K} \quad (13)$$

Consequently, the covariance of the residual term is determined by employing the derivation presented in Equation 10:

$$\Sigma_{\mathbf{r}_D(\mathbf{x}_i, p_k)} = \mathbf{J}_{\mathbf{n}_k} \Sigma_k \mathbf{J}_{\mathbf{n}_k}^T \quad (14)$$

Note that this covariance indicates the “confidence” of one radar point regarding the residual term $\mathbf{r}_D(\cdot)$. For instance, closer radar points are with higher confidence, leading to larger Doppler velocity-aided residuals in the optimization problem and making a more accurate radar SLAM system.

D. Probability-guided Point Matching

Data association, or point matching, plays a pivotal role in point-based scan matching for robotic pose estimation [25].

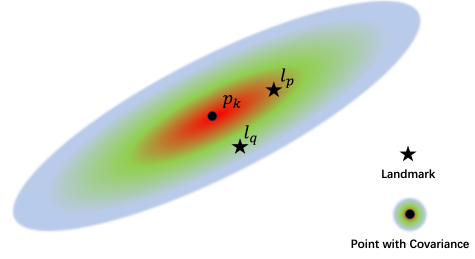


Fig. 3. Given a radar point p_k , the matched map landmark is l_p using our probability-guided point matching approach though l_q is closer under Euclidean distance. The colors represent the probability density.

Prior research has demonstrated the feasibility of tracking radar points across successive radar scans [26]. In our previous study [7], we employed a nearest neighbor-based search within Euclidean space. However, due to the inherent uncertainties in radar point measurements, the proximate points determined by this method do not always correspond to the most probable matches in a statistical sense. As delineated in Section III-B, the probabilistic distribution of radar points within Euclidean space assumes an ellipsoidal shape due to the uncertainty model of the measurements. Thus a shorter Euclidean distance to a central point does not necessarily indicate a higher probability of the point’s presence at that location. This discrepancy suggests that employing a nearest-neighbor search in Euclidean space might lead to mismatches for state estimation.

To address this issue, we propose a probability-guided matching approach with the uncertainty model outlined in Section III-B. This approach involves calculating the probability of a successful match for each point pair, thereby refining the data association step, i.e., point-to-point matching step. This approach aims to mitigate the limitations of traditional nearest-neighbor searches by leveraging the probabilistic distribution of measurement uncertainty into the data association step.

Specifically, for a radar point p_k viewed in polar coordinate attached in current radar pose, a number map landmarks $\mathbf{l}_m \in \mathbf{X}$ could be regarded as candidates. In the matching process, we compute the probability density $P_k(r, \theta, \phi)$ of each candidate landmark around the radar point p_k , as illustrated in Figure 3. In the proposed uncertainty model, r, θ, ϕ are assumed to be mutually independent Gaussian random variables. Thus the matched probability of one landmark $l_q \in \mathbf{l}_m$ is P_k and can be derived as:

$$P_k(l_q) = \frac{1}{\sqrt{(2\pi)^3 |\Sigma_k|}} e^{-\frac{1}{2}(l_q - p_k)^T \Sigma_k^{-1} (l_q - p_k)} \quad (15)$$

then the matched landmark that we are looking for is the one with the largest probability, stated as follows:

$$p_{\text{paired}} = \arg \max_{\mathbf{l}_m} P_k(l_q) \quad (16)$$

Despite the probability-guided point matching, we will also verify whether p_{paired} is within the expected range using the 3-sigma rule. Points that do not fit within this range are considered outliers and removed. Upon the removal of dynamic points, point pairs are computed utilizing the aforementioned method, which facilitates the establishment of correspondence between sequential frames.

E. Uncertainty-aware Residual on Point Matching

Finally, with the estimated point matching in Section III-D, we formulate the point-to-point residual term $r_P(\cdot)$ as follows:

$$\mathbf{r}_P(\mathbf{x}_i, \mathbf{l}_k, p_k) = \mathbf{l}_k - (\mathbf{R}_i(\mathbf{R}_E p_k + \mathbf{t}_E) + \mathbf{p}_i) \quad (17)$$

where \mathbf{l}_k is the position of the matched landmark; p_k is the observed point of \mathbf{l}_k in the i -th scan. The residual is formulated by considering the distance between the landmark and the measurement point corresponding to it.

The inclusion of the noise term \mathbf{n}_k results in the formulation:

$$\begin{aligned} 0 &= \mathbf{l}_k - (\mathbf{R}_i(\mathbf{R}_E(p_k + \mathbf{n}_k) + \mathbf{t}_E) + \mathbf{p}_i) \\ &\approx \mathbf{r}_P(\mathbf{x}_i, \mathbf{l}_k, p_k) + \mathbf{J}_{\mathbf{n}_k} \mathbf{n}_k \end{aligned} \quad (18)$$

in which the term $\mathbf{r}_P(\cdot)$ refers to the residual on point-to-point matching, while \mathbf{n}_k represents the noise of one radar point measurement p_k . The term $\mathbf{J}_{\mathbf{n}_k}$ can be derived as follows:

$$\mathbf{J}_{\mathbf{n}_k} = \mathbf{R}_i \mathbf{R}_E \quad (19)$$

then, the covariance for residual weighting is:

$$\Sigma_{\mathbf{r}_P(\mathbf{x}_i, \mathbf{l}_k, p_k)} = \mathbf{J}_{\mathbf{n}_k} \Sigma_k \mathbf{J}_{\mathbf{n}_k}^T \quad (20)$$

Similar to the aforementioned residual $\mathbf{r}_D(\cdot)$, each radar point is with different noise, thus the proposed uncertainty model results in the adjustment of weights that are assigned to the residual $\mathbf{r}_P(\cdot)$.

To this end, we have proposed our models and approaches that could answer the two questions in Section I: *How to model the uncertainty of radar measurements?* (Section III-B) and *How to incorporate the uncertainty modeling into a radar SLAM system effectively?* (Section III-C, III-D and III-E). We conduct real-world experiments to validate the proposed approaches in the following experimental sections.

IV. EXPERIMENTS

This section details the experimental validation, including the experimental setup, ablation studies, and numerical evaluations alongside comparative analyses.

A. Experimental Setup

We conduct experiments on two different datasets: one is our self-collected dataset on a mobile platform, shown in Figure 4, and the other is the public Radar dataset ColoRadar [8]. Our platform consists of a 4D FMCW Radar ARS548RDI manufactured by Continental and an IMU BMI088 manufactured by Bosch. The radar sensor is mounted on the front of the platform, while the IMU is mounted on the bottom. To obtain precise ground truth poses for evaluation, we employ a motion capture system. This system allowed us to collect three distinct sequences for evaluation, each presenting varying levels of difficulty. Sequence 1 involved relatively low-speed movements, serving as a baseline for comparison. Sequence 2 was collected at higher speeds, introducing additional challenges. Lastly, Sequence 3 was the most challenging, characterized by high rotation and translation speeds.

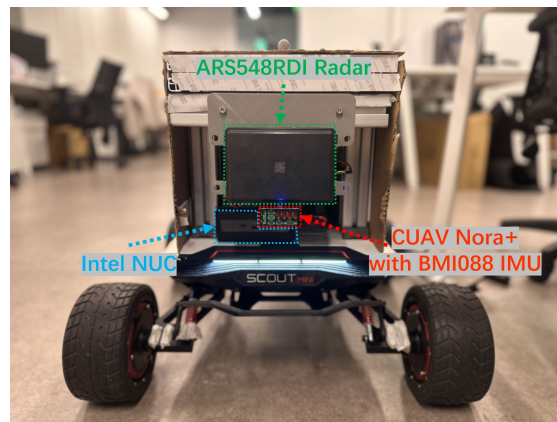


Fig. 4. Our customized vehicle for experimental validation. The vehicle includes the radar sensor, IMU and computing platform. We validate our proposed modeling and methodologies within a controlled room outfitted with a motion capture system.

As for the ColoRadar dataset, we select several sequences for evaluation. The ColoRadar dataset consists of data collected by a single-chip Texas Instruments AWR1843BOOST-EVM radar sensor paired with a DCA1000-EVM for raw data capture. We specifically chose the indoor sequence “12_21_2020_arpg_lab_run0” referred to as “ColoRadar 1”, and the outdoor sequence “2_28_2021_outdoor_run0” referred to as “ColoRadar 2”. The ColoRadar 1 was collected in a lab environment with a motion capture system providing ground truth. The ColoRadar 2 was collected in an outdoor environment with high-precision LiDAR Odometry as the ground truth. Both sequences were acquired using a hand-held platform with aggressive motion, posing significant challenges to the radar odometry system.

It is worth noting that the sensor characteristics of these two datasets are different. Thus the covariance settings also vary. In our self-collected dataset, we set the 3-sigmas of Gaussians equal to the “largest detection errors” provided by the sensor datasheet, thus obtaining the values of σ_r and Σ_Ω . The ColoRadar does not provide such parameters for uncertainty modeling. To address this, we fine-tune the covariances using the ColoRadar 1 sequence and then apply the same parameters to the ColoRadar 2 sequence. Additionally, in the previous study [7], we enhance the radar-inertial odometry with the radar cross-section information, which is a type of intensity of radar points. In this study, we disable all the physical-enhanced modules and test the proposed approaches clearly and thoroughly.

B. Do We Need to Model the Uncertainty?

We compare the full system with several uncertainty-eliminated versions, i.e., setting σ_r or Σ_Ω to a very small value. Essentially, this will affect the weights assigned to the residuals in the optimization process, leading to different motion estimation results. To evaluate the ablated systems, we conducted tests using four sequences that encompassed indoor and outdoor scenes with varying platform speeds. Table I and Figure 6 present the quantitative results and the motion trajectories, respectively.

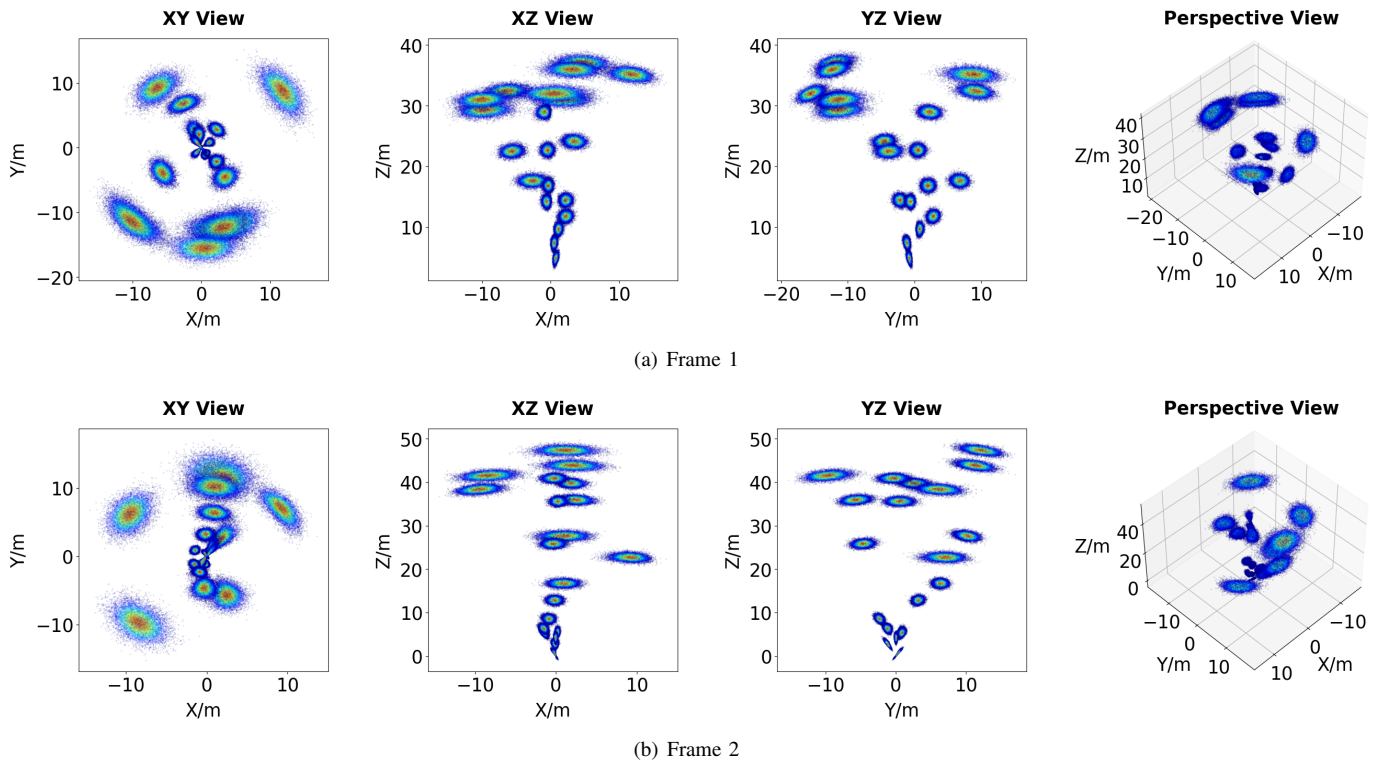


Fig. 5. Visualization of the 3σ ellipse in Cartesian coordinates, and $(0, 0, 0)$ is the coordinates of the radar sensor. We present two frames for better understanding of the proposed uncertainty model. The colors represent the probability density.

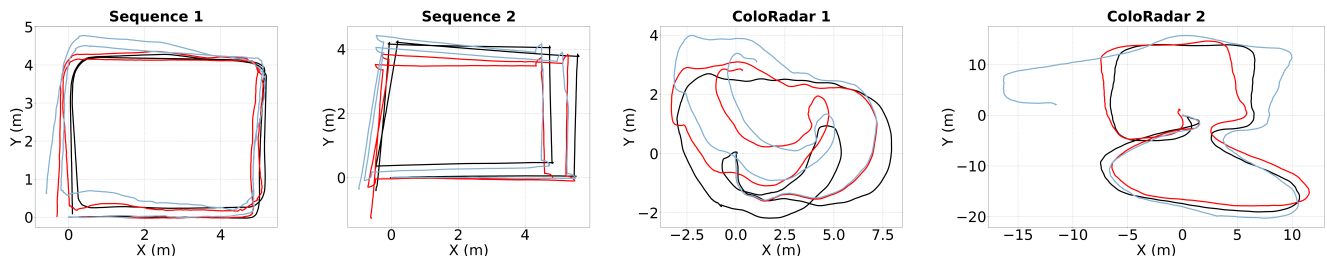


Fig. 6. Trajectories compared with the ground truth: **Red** trajectory is the proposed full system. **Blue** one is the system without uncertainty model, and black one is the ground truth trajectory. We present the results on four sequences in two different datasets.

The experimental results demonstrate that incorporating uncertainty measurement in the system leads to superior performance in terms of most evaluation metrics across various sequences. Systems without modeled uncertainty or with partial implementation exhibit inferior performance in comparison. This finding highlights the necessity of the uncertainty model and also validates the effectiveness of the incorporating scheme proposed in this study.

Despite the ablated studies above, we also test the proposed data association approach individually. We compare our approach with the Euclidean distance-based nearest neighbor search, which is a widely used approach for range sensing-based SLAM systems. As shown in Figure 7, our approach has an overall improvement compared to the Euclidean-based, thus validating the effectiveness of the proposed uncertainty model and probability-guided point matching.

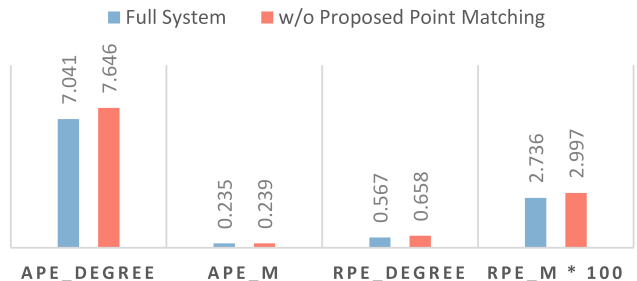


Fig. 7. The ablated studies on the proposed probability-guided point matching. The radar SLAM performs better if the proposed matching is integrated in the system.

C. Is the Parameter Right?

As mentioned in Section IV-A, the covariance settings are directly based on the radar datasheet when using our self-

TABLE I
QUANTITATIVE RESULTS OF ABLATION STUDY
ON UNCERTAINTY MODELING (UM)

Sequence	method	APE RMSE		RPE RMSE	
		Trans.(m)	Rot.(°)	Trans.(m)	Rot.(°)
Sequence 1	w/o UM	0.505	11.485	0.032	1.141
	w/o Range UM	0.480	10.087	0.041	1.595
	w/o Agular UM	0.562	10.859	0.045	1.596
	Ours	0.235	7.041	0.027	0.566
Sequence 2	w/o UM	0.333	10.293	0.059	1.101
	w/o Range UM	0.933	20.611	0.067	1.819
	w/o Agular UM	0.956	20.159	0.072	1.763
	Ours	0.586	5.415	0.051	0.818
ColoRadar 1	w/o UM	6.187	22.750	0.045	1.067
	w/o Range UM	6.198	22.988	0.045	1.078
	w/o Agular UM	6.192	22.869	0.045	1.075
	Ours	6.101	12.640	0.044	0.981
ColoRadar 2	w/o UM	9.466	52.867	0.041	2.418
	w/o Range UM	8.063	28.949	0.042	2.581
	w/o Agular UM	11.508	65.591	0.120	2.373
	Ours	7.469	11.983	0.038	2.162

TABLE II
QUANTITATIVE RESULTS OF DIFFERENT SETS OF MODELED
UNCERTAINTY ON SELF-COLLECT DATASET

α	APE RMSE		RPE RMSE	
	Trans.(m)	Rot.(°)	Trans.(m)	Rot.(°)
0.25	2.174	17.102	0.0534	2.390
0.5	1.953	15.119	0.0534	2.295
1	1.791	14.805	0.0522	2.105
1.5	1.585	11.973	0.0541	2.039
2	1.644	12.249	0.0549	2.101
3	1.945	12.783	0.0587	2.334
4	2.495	16.154	0.0656	2.890

collected dataset. In this section, we will examine the pivotal role of uncertainty parameters in the radar SLAM system by changing covariance parameters accordingly. Theoretically, when the covariance parameters are set to relatively large values, more radar points will be assigned with smaller weights in the motion estimation process. Hence, IMU measurements will have a larger impact on motion estimation, even though radar measurements are inherently more accurate. This imbalance can lead to a biased state estimation. On the other hand, if the uncertainty parameters are set to smaller values, it will also lead to a biased estimation. Therefore, finding an appropriate balance and accurately calibrating the uncertainty parameters is crucial to ensure that radar measurements are properly weighted and contribute more effectively to the motion estimation.

To validate our analysis above, we conduct experiments on Sequence 3, and we apply the coefficients to the parameters of uncertainty models (covariances). Specifically, the parameters are changed to $\Sigma = \alpha \Sigma$, where α denotes the coefficient ranging from 0.25 to 4 and $\Sigma = (\sigma_r, \Sigma_\Omega)$. The results are summarized in Table II. To provide a clearer understanding, we also present the results graphically in Figure 8: the normalized root mean square error (RMSE) ranges from 0 to 1, i.e., ranges from the best performance to the worst one.

In Table II and Figure 8, the estimation performance varies when the covariances are either too small or too large. This could support our analysis on the influence of uncertainty. Interestingly, we find that the parameters provided in the radar

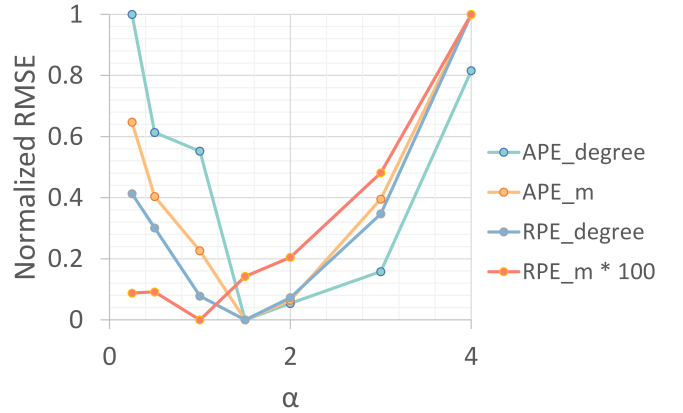


Fig. 8. Normalized RMSE within the range of 0 to 1, and x-axis represents the coefficient α from 0.25 to 4 shown in Table II.

datasheet ($\alpha=1$) tend to yield the best performance. The best performance is achieved when α is in the range of $[1, 1.5]$. We consider that this is mainly due to two reasons. First, the largest error provided by the datasheet is not equal to the 3-sigma in the Gaussian distribution. Further studies on radar sensing are required if we need to obtain the covariance parameters precisely. Second, these parameters on datasheets may not be optimal due to variations among individual radar sensors. It is necessary to calibrate the covariance parameters to achieve better performance. In summary, the parameters (largest detection errors) from the datasheet are critical for modeling point uncertainty in the radar SLAM, and they could help improve the performance of the estimation system. Further studies are required to precisely estimate such parameters via deep analyses and real-world tests.

D. Performance Evaluation of Uncertainty-aware RIO

We compare the complete RIO system with other radar SLAM systems in terms of accuracy. The competitive methods include EKF-RIO [19], Point-to-Distribution (P2D), and Distribution-to-Multi-Distribution (D2M) [6]. EKF-RIO is a widely recognized open-source radar-inertial odometry system, and we adopt the EKF-RIO system using the open-source version. P2D and D2M share similarities with ours in terms of point correspondences and residuals but differ in their approaches. P2D utilizes commonly used laser-scan matching techniques. D2M builds a distribution for each current point by searching for neighboring points. We implement the P2D and D2M methods by ourselves. Additionally, we follow the guidelines presented in the respective papers [6] to enhance their performance by constructing submaps.

The experimental results are summarized in Table III. In the self-collected sequences, our system achieves better performance on the RMSE metrics. Specifically, in terms of Absolute Pose Error (APE) RMSE, our system outperforms the other methods significantly. In the ColoRadar dataset, which is collected using a single-chip radar sensor, the presence of radar measurement noise presents challenges for all systems. EKF-RIO, in this case, exhibits instability due to discarding too many radar measurements. It occasionally provides good

TABLE III
QUANTITATIVE RESULTS OF COMPARISON STUDY

Sequence	method	APE RMSE		RPE RMSE	
		Trans.(m)	Rot.(°)	Trans.(m)	Rot.(°)
Sequence 1	EKF-RIO	0.800	15.338	0.114	0.499
	P2D	0.834	8.485	0.069	0.720
	D2M	1.194	21.457	0.027	0.646
	Ours	0.235	7.041	0.027	0.566
Sequence 2	EKF-RIO	2.805	8.835	0.392	0.866
	P2D	0.743	5.677	0.061	0.805
	D2M	87.189	8.345	2.148	0.806
	Ours	0.586	5.415	0.051	0.818
Sequence 3	EKF-RIO	68.960	66.228	2.195	2.111
	P2D	2.021	12.729	0.052	2.241
	D2M	3.277	21.091	0.273	2.411
	Ours	1.791	14.805	0.052	2.105
ColoRadar 1	EKF-RIO	5.348	24.416	0.054	6.044
	P2D	5.964	13.030	0.067	0.77
	D2M	5.993	13.605	0.066	0.743
	Ours	6.101	12.640	0.044	0.981
ColoRadar 2	EKF-RIO	10.692	14.764	0.047	0.497
	P2D	11.159	20.024	0.054	2.098
	D2M	10.642	15.623	0.054	2.079
	Ours	5.993	13.605	0.066	0.7

results, as it could also introduce drift in both translation and rotation. P2D and D2M methods consider the geometry information surrounding radar points for matching. However, due to the noise and sparsity of radar data, the distribution estimation may be incorrect, resulting in occasional larger errors compared to conventional laser scan matching.

V. CONCLUSION

In this study, we model the uncertainty of radar points and incorporate it into the RIO system. Specifically, the uncertainty model is leveraged into building radar point matching and weighting the residual terms for motion estimation. Real-world experiments demonstrate the effectiveness of our proposed approaches, with ablated studies on two different radar sensors. We also present detailed tests and analyses on parameter settings of uncertainty, making the proposed model and approaches interpretable and applicable.

Radar has become a new wave in recent years and has been applied to many robotic applications [27]. Several potential problems are still not solved well. We will focus on several promising directions in the future, such as multi-modal fusion, multi-radar calibration and graph-theoretic data association for robust estimation.

REFERENCES

- [1] T. Qin, P. Li, and S. Shen, "Vins-mono: A robust and versatile monocular visual-inertial state estimator," *IEEE Transactions on Robotics*, vol. 34, no. 4, pp. 1004–1020, 2018.
- [2] B. Jiang and S. Shen, "A lidar-inertial odometry with principled uncertainty modeling," in *2022 IEEE/RSJ International Conference on Intelligent Robots and Systems (IROS)*. IEEE, 2022, pp. 13 292–13 299.
- [3] Z. Hong, Y. Petillot, A. Wallace, and S. Wang, "Radarslam: A robust simultaneous localization and mapping system for all weather conditions," *The International Journal of Robotics Research*, vol. 41, no. 5, pp. 519–542, 2022.
- [4] H. Yin, R. Chen, Y. Wang, and R. Xiong, "Rall: end-to-end radar localization on lidar map using differentiable measurement model," *IEEE Transactions on Intelligent Transportation Systems*, vol. 23, no. 7, pp. 6737–6750, 2021.

- [5] A. Kramer, C. Stahoviak, A. Santamaria-Navarro, A.-a. Aghamohammadi, and C. Heckman, "Radar-inertial ego-velocity estimation for visually degraded environments," in *2020 IEEE International Conference on Robotics and Automation (ICRA)*, 2020, pp. 5739–5746.
- [6] Y. Zhuang, B. Wang, J. Huai, and M. Li, "4d iriom: 4d imaging radar inertial odometry and mapping," *IEEE Robotics and Automation Letters*, 2023.
- [7] Q. Huang, Y. Liang, Z. Qiao, S. Shen, and H. Yin, "Less is more: Physical-enhanced radar-inertial odometry," in *2024 IEEE international conference on robotics and automation (ICRA)*. IEEE, 2024.
- [8] A. Kramer, K. Harlow, C. Williams, and C. Heckman, "Coloradar: The direct 3d millimeter wave radar dataset," 2021.
- [9] M. L. Rodríguez-Arévalo, J. Neira, and J. A. Castellanos, "On the importance of uncertainty representation in active slam," *IEEE Transactions on Robotics*, vol. 34, no. 3, pp. 829–834, 2018.
- [10] H. Yin, S. Li, Y. Tao, J. Guo, and B. Huang, "Dynam-slam: An accurate, robust stereo visual-inertial slam method in dynamic environments," *IEEE Transactions on Robotics*, vol. 39, no. 1, pp. 289–308, 2022.
- [11] W. Zhen, Y. Hu, J. Liu, and S. Scherer, "A joint optimization approach of lidar-camera fusion for accurate dense 3-d reconstructions," *IEEE Robotics and Automation Letters*, vol. 4, no. 4, pp. 3585–3592, 2019.
- [12] D. Belter, M. Nowicki, and P. Skrzypczyński, "Improving accuracy of feature-based rgb-d slam by modeling spatial uncertainty of point features," in *2016 IEEE international conference on robotics and automation (ICRA)*. IEEE, 2016, pp. 1279–1284.
- [13] S. Thrun, "Probabilistic robotics," *Communications of the ACM*, vol. 45, no. 3, pp. 52–57, 2002.
- [14] T. D. Barfoot, *State estimation for robotics*. Cambridge University Press, 2024.
- [15] M. Shan, Q. Feng, and N. Atanasov, "Orcvio: Object residual constrained visual-inertial odometry," in *2020 IEEE/RSJ International Conference on Intelligent Robots and Systems (IROS)*. IEEE, 2020, pp. 5104–5111.
- [16] N. Merrill, Y. Guo, X. Zuo, X. Huang, S. Leutenegger, X. Peng, L. Ren, and G. Huang, "Symmetry and uncertainty-aware object slam for 6dof object pose estimation," in *Proceedings of the IEEE/CVF Conference on Computer Vision and Pattern Recognition*, 2022, pp. 14 901–14 910.
- [17] C. Yuan, X. Liu, X. Hong, and F. Zhang, "Pixel-level extrinsic self calibration of high resolution lidar and camera in targetless environments," *IEEE Robotics and Automation Letters*, vol. 6, no. 4, pp. 7517–7524, 2021.
- [18] S. Clark and G. Dissanayake, "Simultaneous localization and map building using millimeter wave radar to extract natural features," in *Proceedings 1999 IEEE International Conference on Robotics and Automation (Cat. No. 99CH36288C)*, vol. 2. IEEE, 1999, pp. 1316–1321.
- [19] C. Doer and G. F. Trommer, "An ekf based approach to radar inertial odometry," in *2020 IEEE International Conference on Multisensor Fusion and Integration for Intelligent Systems (MFI)*. IEEE, 2020, pp. 152–159.
- [20] J. Michalczyk, R. Jung, and S. Weiss, "Tightly-coupled ekf-based radar-inertial odometry," in *2022 IEEE/RSJ International Conference on Intelligent Robots and Systems (IROS)*. IEEE, 2022, pp. 12 336–12 343.
- [21] J. Michalczyk, R. Jung, C. Brommer, and S. Weiss, "Multi-state tightly-coupled ekf-based radar-inertial odometry with persistent landmarks," in *2023 IEEE International Conference on Robotics and Automation (ICRA)*. IEEE, 2023, pp. 4011–4017.
- [22] C. X. Lu, M. R. U. Saputra, P. Zhao, Y. Almalioğlu, P. P. De Gusmao, C. Chen, K. Sun, N. Trigoni, and A. Markham, "milliego: single-chip mmwave radar aided egomotion estimation via deep sensor fusion," in *Proceedings of the 18th Conference on Embedded Networked Sensor Systems*, 2020, pp. 109–122.
- [23] K. Retan, F. Loshaj, and M. Heizmann, "Radar odometry on se(3) with constant acceleration motion prior and polar measurement model," 2022.
- [24] D. He, W. Xu, and F. Zhang, "Kalman filters on differentiable manifolds," *arXiv preprint arXiv:2102.03804*, 2021.
- [25] F. Pomerleau, F. Colas, R. Siegwart *et al.*, "A review of point cloud registration algorithms for mobile robotics," *Foundations and Trends® in Robotics*, vol. 4, no. 1, pp. 1–104, 2015.
- [26] J. Zhang, H. Zhuge, Z. Wu, G. Peng, M. Wen, Y. Liu, and D. Wang, "4dradar slam: A 4d imaging radar slam system for large-scale environments based on pose graph optimization," in *2023 IEEE International Conference on Robotics and Automation (ICRA)*, 2023, pp. 8333–8340.
- [27] K. Harlow, H. Jang, T. D. Barfoot, A. Kim, and C. Heckman, "A new wave in robotics: Survey on recent mmwave radar applications in robotics," *arXiv preprint arXiv:2305.01135*, 2023.